Volume 19, Number 2, 2026. pp. 111-121

Jordan Journal of Physics

ARTICLE

Unsteady Free Convection Flow of Fractionalized Maxwell Fluid over an Inclined Vertical Plate with Heat and Mass Transfer

M. Ramzan[a], **Ahmad Shafique**[a], **Shajar Abbas**[a,b], **Mudassar Nazar**[a], **Mukhlisa Soliyeva**[c], **Afnan Al Agha**[d] and **Hakim AL Garalleh**[d]

[a] *Centre for Advanced Studies in Pure and Applied Mathematics, Bahauddin Zakariya University, Multan, Pakistan.*

[b] *AS (Ayub Shah) Institute of Mathematics and Research Centre, Multan, Pakistan.*

[c] *Department of Physics and Teaching Methods, Tashkent State Pedagogical University, Tashkent, Uzbekistan.*

[d] *Department of Mathematical Science, College of Engineering, University of Business and Technology, Jeddah 21361, Saudi Arabia.*

DOI: **https://doi.org/10.47011/19.2.1**

Received on: 25/04/2022; *Accepted on: 29/05/2025*

Abstract: This study examines the unsteady motion of a fractional Maxwell fluid over an inclined vertical surface, considering the effects of thermo-diffusion and slip conditions. The model is further developed using Fick's and Fourier's laws, introducing a novel fractional formulation for mass diffusion and thermal diffusivity. The flow model is formulated with the CPC fractional derivative, and the governing equations are transformed into a non-dimensional form, and the resulting governing equations are solved using the Laplace transform method. The effects of key flow parameters—including the Grashof number, chemical reaction rate, Prandtl number, fractional parameters, and Schmidt number—are analyzed graphically. The results indicate that the fractional model provides a more accurate and flexible description of flow behavior than the classical model. Specifically, the magnetic field suppresses fluid motion, while thermo-diffusion enhances it.

Keywords: Free convection, Maxwell fluid, Slip condition, Soret effect, CPC fractional derivative.

1. Introduction

Recent advancements have significantly improved the understanding and modeling of non-Newtonian fluids, particularly viscoelastic fluids such as Maxwell fluids. These fluids, characterized by their unique combination of elasticity and viscosity, play an important role in numerous engineering and industrial applications. Fractional calculus has been widely used to describe their complex dynamics, incorporating fractional-order differentiation techniques for greater accuracy. In particular, the constant proportional Caputo (CPC) operator has been employed to improve the modeling of heat flux behavior under various physical conditions, including magnetic fields and variable boundaries.

Building on these developments, this study examines the transient behavior of Maxwell fluid using the CPC fractional derivative to provide new insights into viscoelastic fluid dynamics. Previous research has explored similar topics, such as the MHD thermal transfer framework in Maxwell fluid by Kai-Long Hsiao [1], and the effects of fractional calculus on blood flow in cylindrical structures by Shah et al. [2]. The Jeffreys fluid model, widely studied because of its mathematical simplicity, has been analyzed by Shafique et al. [3, 4], while Ahmad et al. [5] examined its fractional-order form using Caputo and Caputo-Fabrizio derivatives. These derivatives emerged over the past decade, among other generalized fractional differentiation

Corresponding Author: M. Ramzan **Email**: muhammadramzan443445@gmail.com

approaches [6, 7].

There has been extensive research conducted on natural convection over inclined surfaces under different thermal and mechanical conditions [8-14]. Fetecau et al. [15] analyzed the unsteady behavior of second-grade fluid near a plate, while Ahmed et al. [16] investigated MHD heat transfer in boundary regions with minimal pressure variations. Narayana [17] explored convective mixed MHD flow, and Nadeem et al. [18] studied MHD flow in an inclined viscoelastic fluid within a convective environment.

Fractional calculus, which extends classical calculus by considering derivatives of arbitrary continuous order, has a long history dating back to Leibniz's correspondence with l'Hôpital in the 17th century. It has since evolved into a powerful tool for modeling complex physical systems. Unlike traditional integer-order derivatives, which often fail to adequately capture real-world fluid behavior, fractional derivatives account for memory effects and non-local interactions. In this study, the Mittag-Leffler kernel fractional derivative is employed, offering a more generalized and flexible framework compared to Caputo and Caputo-Fabrizio derivatives. This approach effectively models fluids with long-term memory and power-law behavior.

Several studies have investigated related magnetohydrodynamic (MHD) and convective transport problems. Olisa [19] analyzed laminar MHD natural convection past a vertical plate, while Khan et al. [20] studied magnetohydrodynamic flow through a porous medium. Seth et al. [21] examined convective behavior over a vertical plate subjected to a temperature gradient. Stability conditions of fractional derivatives were studied by Tran et al. [22], and Tuan et al. [23] applied fractional models to the study of COVID-19 transmission dynamics. Additional studies explored convective MHD flow past a plate with heat sources [24], Casson fluid behavior in confined passages [25], and Brinkman fluid dynamics in channels and over surfaces [26–28]. Viscoelastic fluid flow over vertical plates has also received considerable attention [29–31].

The current study focuses on the unsteady motion of fractional Maxwell fluid across an inclined vertical plate, incorporating slip and Soret effects. The governing equations are transformed into their dimensionless form and solved using the Laplace integral transform method. The resulting velocity, temperature, and concentration profiles are graphically examined to provide a deeper understanding of the fluid's behavior.

2. Mathematical Model

The motion of a fractional Maxwell fluid along an inclined vertical plate is analyzed under the influence of Soret and slippage conditions. The fluid travels upward parallel to the y-axis, while the x-axis remains perpendicular to the plate, which is inclined at an angle A in the vertical plane.

Initially, at $t = 0$, both the fluid and the plate are at rest and maintained at the ambient concentration C_∞ and ambient temperature T_∞. For $t > 0$, the plate begins to move in its own plane at a uniform velocity of $U_1 f(t)$. Simultaneously, the concentration and temperature of the plate increase over time, following the expressions $C_w^{\cdot}\cdot$ and $T^* = T_w^*\left(1 - c_1 e^{-d_1 t}\right) + T_\infty^*$, respectively. Based on these assumptions and following [28, 31], the governing equations are given by:

$$\left(1+\lambda_1\frac{\partial}{\partial t}\right)\frac{\partial u_1(x^*,t)}{\partial t} = \frac{\partial \tau(x^*,\mathrm{t})}{\partial x^*} + \left(1+\lambda_1\frac{\partial}{\partial t}\right) g\beta_{T^*}(T^* - T_\infty^*)\cos(A) + \left(1+\lambda_1\frac{\partial}{\partial t}\right) g\beta_{C^{\cdot}}(C^{\cdot} - C_\infty^{\cdot})\cos(A) - \left(1+\lambda_1\frac{\partial}{\partial t}\right)\frac{\sigma\beta_0^2 u_1(x^*,\mathrm{t})}{\rho} - \left(1+\lambda_1\frac{\partial}{\partial t}\right)\frac{\mu u_1(x^*,\mathrm{t})}{\rho K_2} \tag{1}$$

Shear stress τ is:

$$\tau = \frac{\partial u_1(x^*,t)}{\partial x}. \tag{2}$$

Heat Eq. is:

$$\frac{\partial T^*(x^*,\mathrm{t})}{\partial \mathrm{t}} = -\frac{\partial q(x^*,\mathrm{t})}{\rho C_p\,\partial x^*} + H_1(T^* - T_\infty^*). \tag{3}$$

Fourier's Law, $q_1(x^*,t)$ is:

$$q_1(x^*,t) = -\alpha_0\frac{\partial T^*(x^*,t)}{\partial x^*}. \tag{4}$$

Diffusion Eq. is:

$$\frac{\partial C^{\cdot}(x^*,\mathrm{t})}{\partial \mathrm{t}} = -\frac{\partial J(x^*,t)}{\partial x^*} - \frac{D_{KT}}{Tm}\frac{\partial q(x^*,\mathrm{t})}{\partial x^*} - S_1(T^* - T_\infty^*). \tag{5}$$

Fick's Law, $J_1(x^*,t)$ is:

$$J_1(x^*,\mathrm{t}) = -D_m\frac{\partial C^{\cdot}(x^*,t)}{\partial x^*}. \tag{6}$$

The conditions for the initial value problem are:

$$u_1(x^*,\mathrm{t}) = 0,\ T(x^*,t) = T_\infty,\ C^{\cdot}(x^*,t) = C_\infty,\ x^* > 0,\ \mathrm{t} = 0, \tag{7}$$

$$u_1(0,\mathrm{t}) - R_1\frac{\partial u_1}{\partial x^*} = U_1 f(t), T^{\cdot}(0,\mathrm{t}) = T_\infty^* + T_w^*\left(1 - c_1 e^{-d_1\mathrm{t}}\right), C^{\cdot}(0,\mathrm{t}) = C_w^{\cdot},\ \mathrm{t} > 0, \tag{8}$$

$$u_1(x^*,t) \to 0, T^*(x^*,\mathrm{t}) \to 0, C^*(x^*,\mathrm{t}) \to 0,\ x^* \to \infty,\ t > 0. \tag{9}$$

3. Generalized Model

To extend the classical Maxwell fluid framework, a generalized framework is developed incorporating fractional derivatives to account for memory effects and nonlocal interactions. The governing equations are reformulated using the CPC fractional derivative, providing a more accurate representation of viscoelastic fluid behavior. This section presents the mathematical formulation of the model, emphasizing the impact of dimensionless parameters on heat and mass transfer.

The nondimensional variables are defined as follows:

$$x^* = \frac{Ux}{\nu},\ t^* = \frac{U^2 t}{\nu},\ T^* = \frac{T^* - T_\infty^*}{T_w^* - T_\infty^*},\ u^* = \frac{u_1}{U}, \mathrm{Gr}^* = \frac{\nu\beta_{T^*}(T_w^* - T_\infty^*)}{U^3},\ C^* = \frac{C^* - C_\infty^*}{C_w^* - C_\infty^*},\ \mathrm{Gm}^* = \frac{\nu\beta_{C^*}(C_w^{\cdot} - C_\infty^*)}{U^3}. \tag{10}$$

Eq. (1) is fractionally generalized by [32]:

$$\tau = L_\beta D_t^\beta \frac{\partial u(x,t)}{\partial x},\ 1 \geq \beta > 0, \tag{11}$$

Substitute Eq. (11) into Eq. (1) and utilize the dimensionless values from Eq. (10).

$$\left(1 + \lambda\frac{\partial}{\partial t}\right)\frac{\partial u(x,t)}{\partial t} = L_\beta D_t^\beta \frac{\partial^2 \bar{u}(x,t)}{\partial x^2} - \left(1 + \lambda\frac{\partial}{\partial t}\right)(K^{-1} + M)u(x,t) + \left(1 + \lambda\frac{\partial}{\partial t}\right)\mathrm{Gr}\, T(x,t)\cos(A) + \left(1 + \lambda\frac{\partial}{\partial t}\right)\mathrm{Gm}\, C(x,t)\cos(A). \tag{12}$$

Equation (2) is fractionally generalized by [33, 34]:

$$q = -B_\gamma D_t^\gamma \frac{\partial T(x,t)}{\partial x}, \tag{13}$$

Substituting Eq. (13) into Eq. (2),

$$\frac{\partial T(x,t)}{\partial t} = \frac{1}{\mathrm{Pr}} D_t^\gamma \frac{\partial^2 T}{\partial x^2} + HT, \tag{14}$$

where $\mathrm{Pr} = \frac{\rho\nu C_P}{B_\gamma}$.

By Fick's Law, Eq. (3) is:

$$J = -C_\alpha D_t^\alpha \frac{\partial C(x,t)}{\partial x},\ 1 \geq C_\alpha > 0, \tag{15}$$

Substituting Eq. (15) into Eq. (3),

$$\frac{\partial C(x,t)}{\partial t} = \frac{1}{\mathrm{Sc}} D_t^\alpha \frac{\partial^2 C(x,t)}{\partial x^2} + SC(x,t) + \mathrm{Sr}\, D_t^\gamma \frac{\partial^2 T(x,t)}{\partial x^2}, \tag{16}$$

where $\mathrm{Sc} = \frac{\nu}{C_\alpha}$.

Conditions are:

$$u(x,t) = 0, T(x,t) = 0, C(x,t) = 0,\ t = 0, x > 0 \tag{17}$$

$$u(0,t) - R\frac{\partial u}{\partial x} = f(t), T(0,t) = 1 - ce^{-dt},\ C(0,t) = t, t > 0, \tag{18}$$

$$u(x,t) \to 0,\ T(x,t) \to 0,\ C(x,t) \to 0,\ x \to \infty, t > 0, \tag{19}$$

The parameters u and t represent fluid motion and time, respectively, while G_r and G_m denote the thermal and mass Grashof numbers. Additionally, *M, H,* and *R* correspond to the magnetic field, dimensionless heat generation parameter, and slip parameter. The quantities Sc, Pr, and Sr represent the Schmidt number, Prandtl number, and Soret parameter, respectively, with T and C denoting temperature and concentration. The term $D_t^\beta u(x,t)$ signifies the CPC derivative, expressed as:

$$D_t^\beta u(x,t) = \frac{1}{\Gamma(1-\beta)}\int_0^t \left[K_1(\beta)u(x,\tau) + K_0(\beta)u'(x,\tau)\right](t-\tau)^{-\beta} d\tau. \tag{20}$$

4. Solution of the Problem

The system of Eqs. (12), (14), and (16), along with the associated boundary conditions, are solved using the Laplace integral transform method.

4.1 Calculation of Temperature

From Eq. (14),

$$s\bar{T}(x,s) = \frac{1}{\mathrm{Pr}}\left[\frac{K_1(\gamma)}{s} + K_0(\gamma)\right] s^\gamma \frac{\partial^2 \bar{T}(x,s)}{\partial x^2} + H\bar{T}(x,s). \tag{21}$$

with

$$\bar{T}(0,s) = \frac{1}{s} - \frac{c}{s+d},\ \bar{T}(x,s) \to 0, x \to \infty. \tag{22}$$

Substitute Eq. (22) into Eq. (21)

$$\bar{T}(x,s)=\left(\frac{1}{s}-\frac{a}{s+b}\right)e^{-x\sqrt{\frac{P_r(s-H)}{\left(\frac{K_1(\gamma)}{s}+K_0(\gamma)s^{\gamma}\right.}}}. \tag{23}$$

4.2 Calculation of Concentration

Taking Laplace transform on Eq. (16) on both sides, we get

$$s\bar{C}(x,s)=\frac{1}{\mathrm{Sc}}\left[\frac{K_1(\alpha)}{s}+K_0(\alpha)\right]s^{\alpha}\frac{\partial^2\bar{C}(x,s)}{\partial x^2}+S\bar{C}(x,s)+\mathrm{Sr}\left[\frac{K_1(\gamma)}{s}+K_0(\gamma)\right]s^{\gamma}\frac{\partial^2\bar{T}(x,s)}{\partial x^2}. \tag{24}$$

with

$$\bar{C}(0,s)=s^{-2},\ \bar{C}(x,s)\to 0, x\to\infty. \tag{25}$$

Utilising Eq. (25) in Eq. (24),

$$\bar{C}(x,s)=\left[s^{-2}+\frac{\mathrm{SrScPr}(s-H)\left(\frac{1}{s}-\frac{c}{s+d}\right)}{(s-H)\mathrm{Pr}-(s+S)\mathrm{Sc}}\right]e^{-x\sqrt{\frac{K_1(\alpha)}{\left[\frac{K_1}{s}+K_0(\alpha)\right]s^{\alpha}}}}-\frac{\mathrm{SrScPr}(s-H)\left(\frac{1}{s}-\frac{c}{s+d}\right)}{(s-H)\mathrm{Pr}-(s+S)\mathrm{Sc}}e^{-x\sqrt{\left[\frac{K_1(\alpha)}{s}+K_0(\alpha-H)\right]s^{\alpha}}}. \tag{26}$$

4.3 Calculation of Velocity

Taking Laplace transform on Eq. (12) on both sides, we get:

$$(1+\lambda s)\bar{u}(x,s)=L_{\beta}\left[\frac{K_1(\beta)}{s}+K_0(\beta)\right]s^{\beta}\frac{\partial^2\bar{u}(x,s)}{\partial x^2}-(1+\lambda s)(K^{-1}+M)\bar{u}(x,s)+(1+\lambda s)\,\mathrm{Gr}\,\bar{T}(x,s)\cos(A)+(1+\lambda s)\,\mathrm{Gm}\,\bar{C}(x,s)\cos(A), \tag{27}$$

with

$$\bar{u}(0,s)-R\frac{\partial\bar{u}(0,s)}{\partial x}=f(s),\ \bar{u}(x,s)\to 0,\ x\to\infty. \tag{28}$$

Substituting Eq. (28) in Eq. (27),

$$\bar{u}(x,s)=\frac{\frac{1}{s^{c+1}}}{1+R\sqrt{\frac{(s+K^{-1}+M)(1+\lambda s)}{L_{\beta}\left[\frac{K_1(\alpha)}{s}+K_0(\alpha)\right]s^{\alpha}}}}e^{-x\sqrt{\frac{(s+K^{-1}+M)(1+\lambda s)}{L_{\beta}\left[\frac{K_1(\alpha)}{s}+K_0(\alpha)\right]s^{\alpha}}}}+(1+\lambda s)\cos(A)\left[\frac{1}{s}-\frac{c}{s+d}\right]\Bigg[\frac{\mathrm{Gr}-\frac{\mathrm{PrScGmSr}(s-H)}{\mathrm{Pr}(s-H)-(s+S)\mathrm{Sc}}}{L_{\beta}\,\mathrm{Pr}(s-H)-(s+k^{-1}+M)(1+\lambda s)}\Bigg]\times$$

$$\Bigg[\frac{1+R\sqrt{\frac{\mathrm{Pr}(s-H)}{\left[\frac{K_1(\alpha)}{s}+K_0(\alpha)\right]s^{\alpha}}}}{1+R\sqrt{\frac{(s+K^{-1}+M)(1+\lambda_s)}{L_{\beta}\left[\frac{K_1(\alpha)}{s}+K_0(\alpha)\right]s^{\alpha}}}}e^{-x\sqrt{\frac{(s+K^{-1}+M)(1+\lambda s)}{L_{\beta}\left[\frac{K_1(\alpha)}{s}+K_0(\alpha)s^{\alpha}\right.}}}-e^{\sqrt{\frac{K_1(\alpha,s-H)}{\left[\frac{K_1(\alpha)}{s}+K_0(\alpha)\right]s^{\alpha}}}}\Bigg]+$$

$$\Bigg[\frac{(1+\lambda s)\cos(A)\left[\frac{\mathrm{Gm}}{s^2}+\left[\frac{1}{s}-\frac{c}{s+d}\right]\right]\frac{\mathrm{PrScGmSr}(s-H)}{\mathrm{Pr}(s-H)-(s+S)\mathrm{Sc}}}{L_{\beta}(s+S)\mathrm{Sc}-(s+k^{-1}+M)(1+\lambda s)}\Bigg]\times$$

$$\Bigg[\frac{1+R\sqrt{\frac{(s+S)\mathrm{Sc}}{\left[\frac{K_1(\alpha)}{s}+K_0(\alpha)\right]s^{\alpha}}}}{1+R\sqrt{\frac{(s+K^{-1}+M)(1+\lambda s)}{L_{\beta}\left[\frac{K_1(\alpha)}{s}+K_0(\alpha)\right]s^{\alpha}}}}e^{-x\sqrt{\frac{(s+K^{-1}+M)(1+\lambda s)}{L_{\beta}\left[\frac{K_1(\alpha)}{s}+K_0(\alpha)\right]s^{\alpha}}}}-e^{\sqrt{\frac{(s+S)\mathrm{Sc}}{\left[\frac{K_1(\alpha)}{s}+K_0(\alpha)\right]s^{\alpha}}}}\Bigg]. \tag{29}$$

5. Results and Discussion

The solution describing Maxwell fluid motion over a vertical surface, including thermo-diffusion and heat-source effects, was derived using the Laplace integral transform method. The influence of various parameters in the governing equations across the velocity, temperature, and concentration fields was analyzed graphically.

Fig. 1(a) illustrates the effect of the thermal Grashof number Gr on the velocity $u(x,t)$, indicating that an increase in Gr leads to a higher fluid velocity. This is attributed to the stronger buoyancy force relative to viscous forces, which enhances buoyancy-driven flow and, consequently, the fluid's motion. Fig. 1(b) shows the effect of Gr on $u(x,t)$ with slip conditions, where the velocity increase is slightly lower than the no-slip case due to reduced momentum transfer at the slipping boundary.

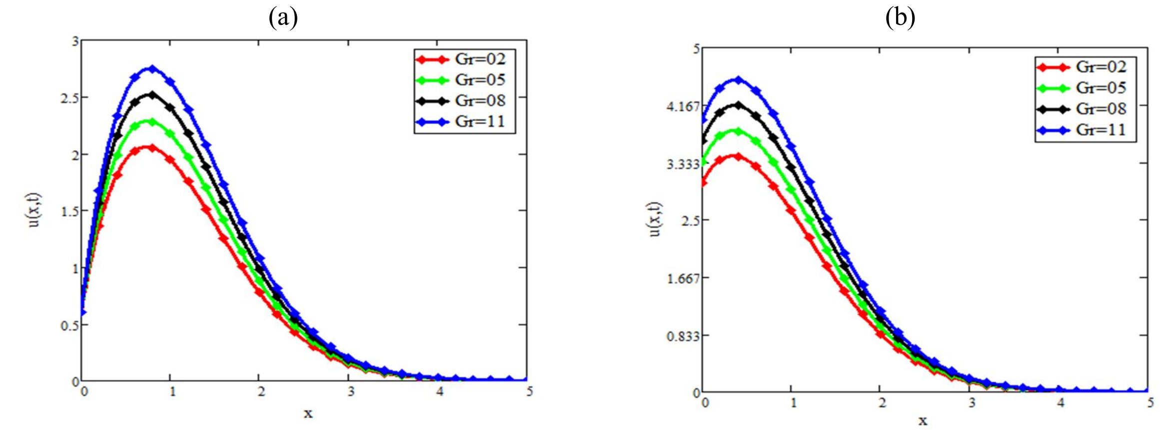

FIG. 1. Velocity profile $u(x,t)$ for different values of the thermal Grashof number (Gr) at $\lambda = 0.6$, Sr = 0.5, M = 0.3, K = 3.5, Sc = 6.2, $G_m = 10$: (a) R = 0.0 and (b) R = 0.6.

Figure 2(a) illustrates the effect of the mass Grashof number (G_m) on the velocity profile $u(x,t)$ under no-slip conditions. It is observed that an increase in G_m enhances the concentration induced buoyancy force, which consequently accelerates the fluid motion and increases the velocity field.

Figure 2(b), presents the influence of G_m under slip conditions. Although the velocity still increases with increasing G_m, the slip condition reduces the influence of buoyancy compared to the no-slip case due to the weaker interaction between the fluid and the surface.

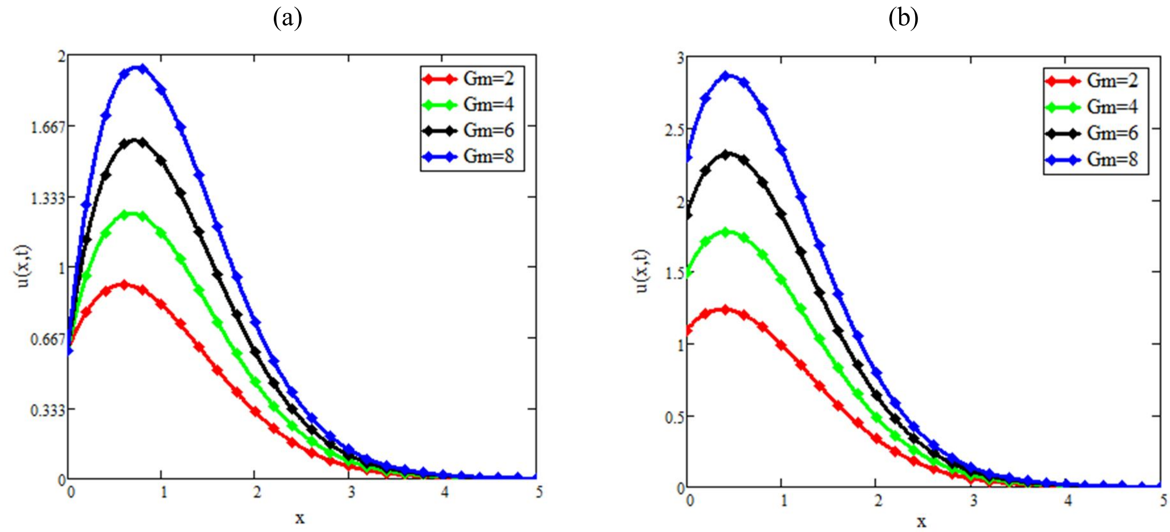

FIG. 2. Velocity profile $u(x,t)$ for different values of G_m at $\lambda = 0.6$, Sr = 0.5, M = 0.3, K = 3.5, Sc = 6.2, Gr = 5: (a) R = 0.0 and (b) R = 0.6.

Figure 3(a) illustrates the effect of the Maxwell parameter (λ) on the velocity profile $u(x,t)$ under no-slip conditions. It is observed that the fluid velocity increases as λ decreases. This behavior occurs because lower values of the Maxwell parameter reduce the fluid's relaxation effects, thereby enhancing the fluid motion.

Figure 3(b) presents the influence of λ on $u(x,t)$ under slip conditions. Although a decrease in λ still leads to an increase in velocity, the enhancement is less pronounced due to partial momentum transfer at the boundary surface.

(a) (b)

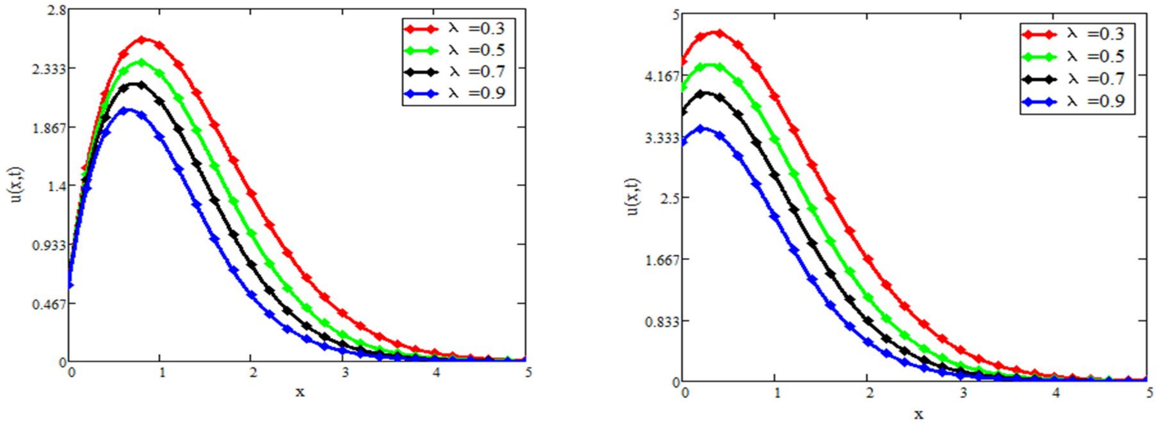

FIG. 3. Velocity profile $u(x,t)$ for different values of G_m at λ = 0.6, Sr = 0.5, M = 0.3, K = 3.5, Sc = 6.2, Gr = 5, G_m = 10: (a) R = 0.0 and (b) R = 0.6.

Figure 4(a) analyzes the influence of the permeability parameter (K)(K)(K) on the velocity profile u(x,t)u(x,t)u(x,t) under no-slip conditions. The results indicate that the fluid velocity decreases as KKK decreases. This behavior is attributed to the reduced permeability of the porous medium, which increases the resistance to fluid motion and consequently suppresses the velocity field.

Figure 4(b) illustrates the effect of K on $u(x,t)$ under slip conditions. A similar reduction in velocity is observed with decreasing K; however, the decline is less pronounced than in the no-slip case due to partial slip at the boundary surface, which weakens the fluid-surface interaction.

(a) (b)

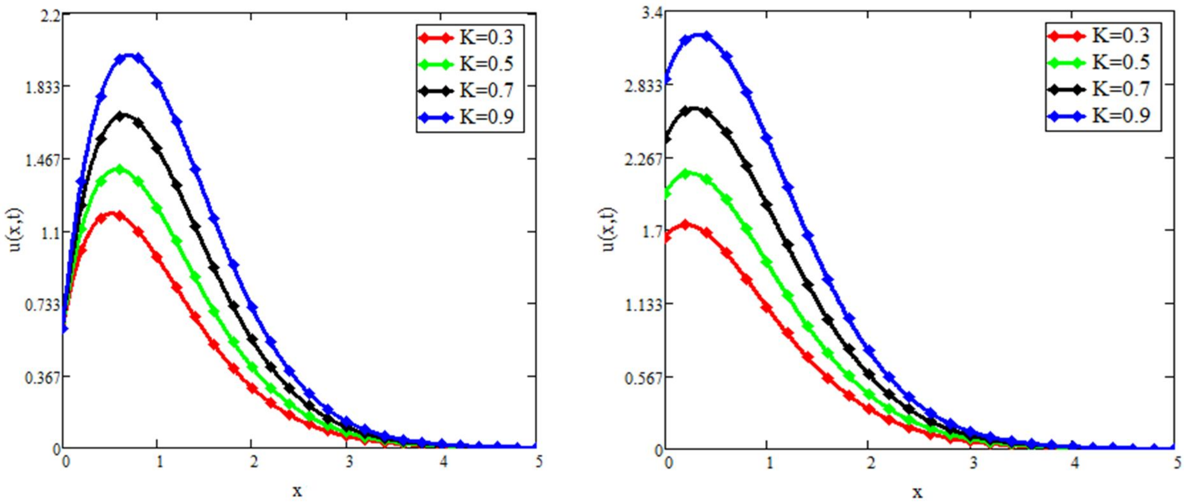

FIG. 4. Velocity profile $u(x,t)$ for different values of K at λ = 0.6, Sr = 0.5, M = 0.3, K = 3.5, Sc = 6.2, Gr = 5, G_m = 10: (a) R = 0.0 and (b) R = 0.8.

Figure 5(a) presents the influence of the magnetic parameter(M) on the velocity profile $u(x,t)$ under no-slip conditions. It is observed that an increase in M leads to a reduction in fluid velocity due to the resistive Lorentz force generated by the applied magnetic field.

Figure 5(b) examines the effect of M under slip conditions. Although the velocity continues to decrease with increasing MMM, the reduction is less pronounced than in the no-slip case because the slip condition permits partial fluid motion along the boundary surface despite the strengthening magnetic field.

(a) (b)

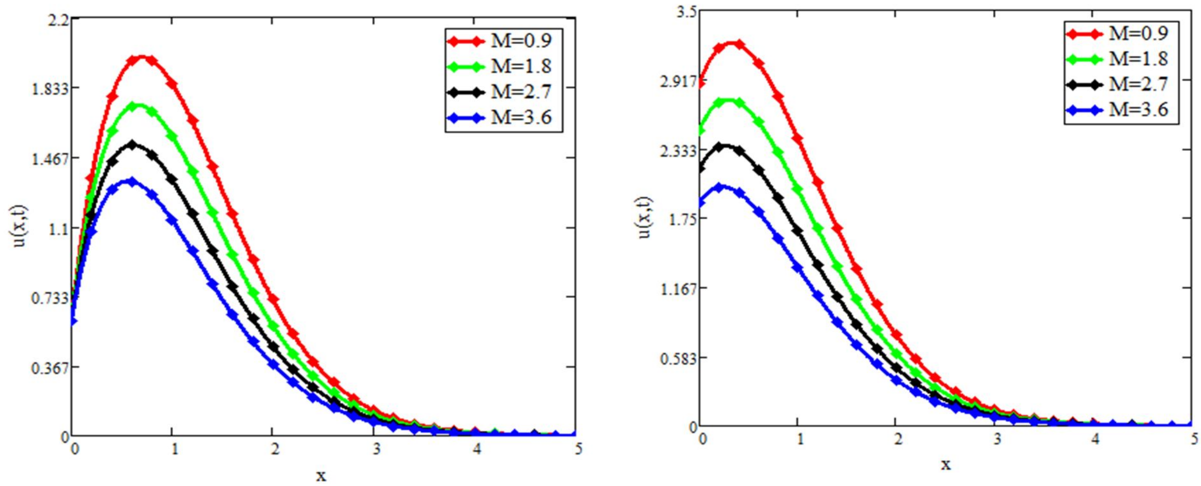

FIG. 5. Velocity profile $u(x,t)$ for different values of M at λ = 0.6, Sr = 0.5, M = 0.3, K = 3.5, Sc = 6.2, Gr = 5, G_m = 10, Gr = 5: (a) R = 0.0 and (b) R = 0.8.

Figure 6(a) illustrates the effect of the Soret parameter (Sr) on the velocity profile $u(x,t)$ under no-slip conditions. The results indicate that the fluid velocity increases with increasing Sr, as the thermo-diffusion effect enhances concentration gradients and strengthens the concentration-induced buoyancy force.

Figure 6(b) presents the influence of Sr under slip conditions. Although the velocity continues to increase with higher values of Sr, the enhancement is less pronounced than in the no-slip case due to the reduced transmission of momentum and boundary forces caused by the slip condition.

(a) (b)

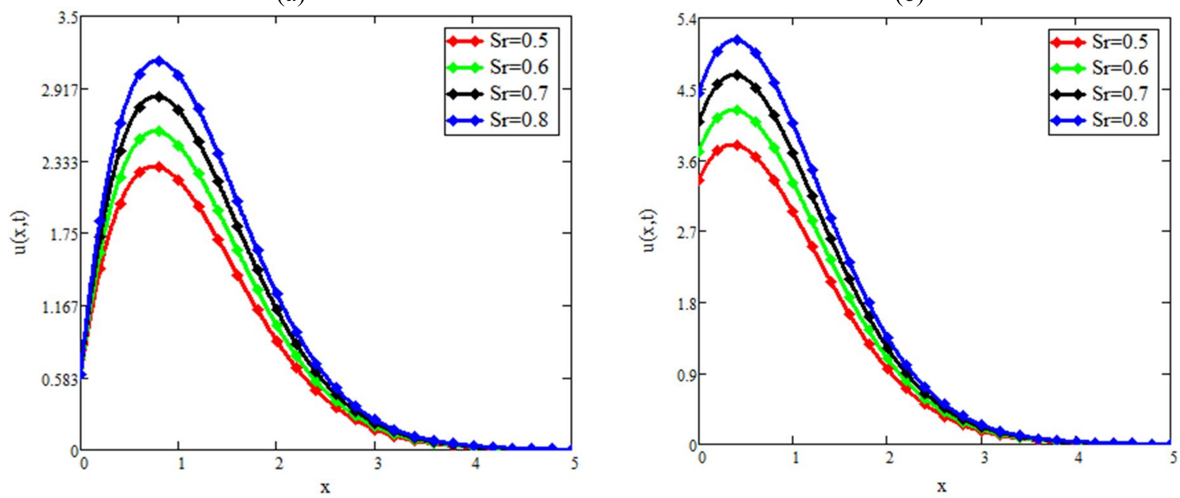

FIG. 6. Velocity profile $u(x,t)$ for different values of Sr at λ = 0.6, M = 0.3, K = 3.5, Sc = 6.2, Gr = 5 G_m = 10, Gr = 5: (a) R = 0.0 and (b) R = 0.8.

Figure 7(a) presents the influence of the inclination angle parameter (A) on the velocity profile $u(x,t)$ under no-slip conditions. The results show that the fluid velocity increases as AAA decreases. This behavior occurs because a smaller inclination angle enhances the component of the buoyancy force acting along the surface, thereby accelerating the fluid motion.

Figure 7(b) illustrates the effect of AAA under slip conditions. Although the velocity still increases with decreasing AAA, the enhancement is less pronounced compared to the no-slip case because the slip condition reduces momentum transfer between the fluid and the boundary surface.

(a) (b)

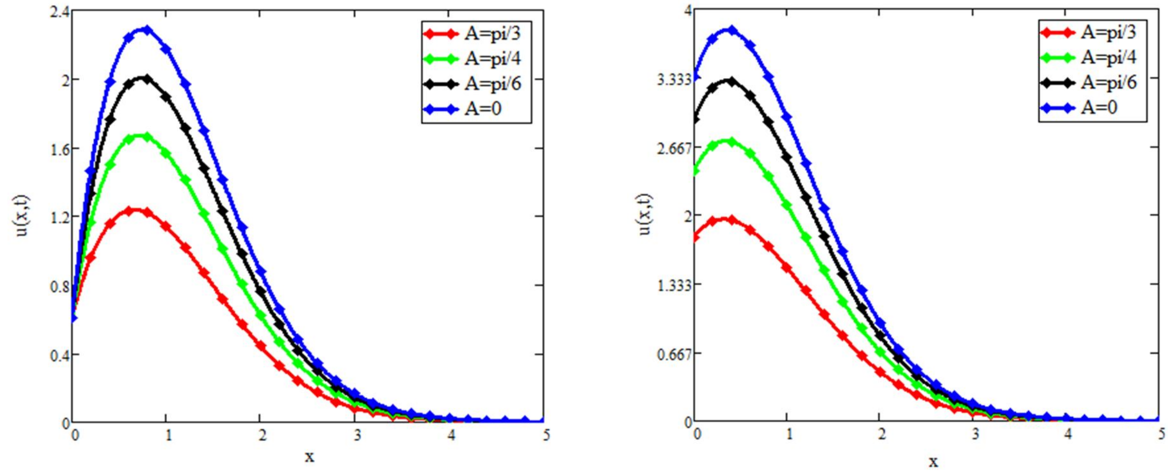

FIG. 7. Velocity profile $u(x,t)$ for different values of angle (A) at λ = 0.6, M = 0.3, K = 3.5, Sc = 6.2, Gr = 5, G_m = 10, Gr = 5: (a) R = 0.0 and (b) R = 0.8.

Figure 8(a) illustrates the influence of the Prandtl number (P_r) on the temperature profile $T(x,t)$. Higher values of P_r correspond to lower thermal diffusivity, resulting in steeper temperature gradients and a thinner thermal boundary layer. In this case, heat diffusion within the fluid is reduced, causing thermal energy to remain concentrated near the surface. Conversely, lower values of P_r enhance thermal diffusion, leading to a more uniform temperature distribution throughout the fluid.

Figure 8(b) presents the effect of the heat generation parameter (H) on $T(x,t)$. The results indicate that increasing H raises the fluid temperature due to enhanced internal energy generation within the fluid. This effect is particularly important in applications involving chemical reactions and combustion processes where heat generation significantly influences thermal behavior.

(a) (b)

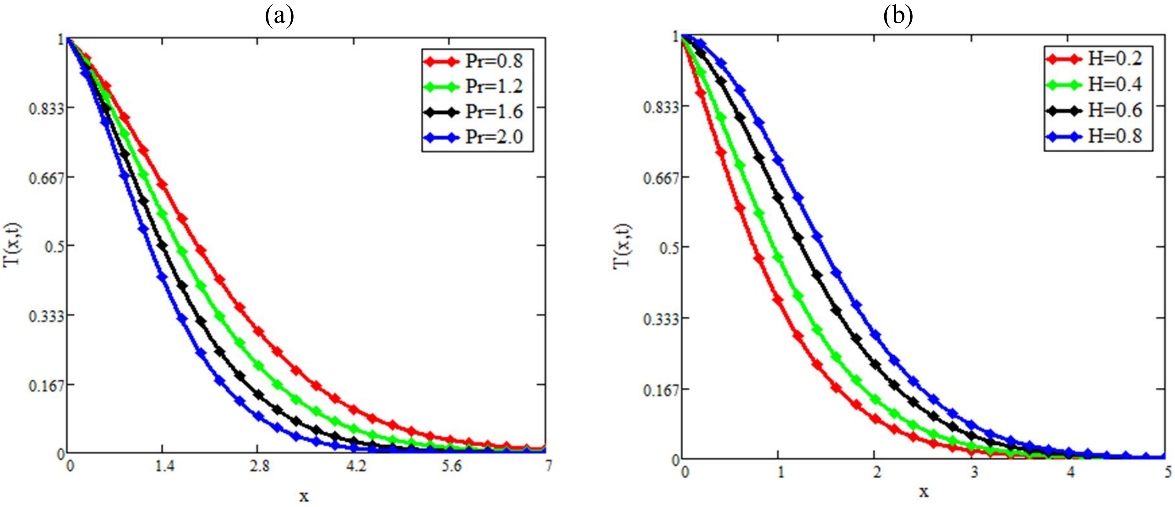

FIG. 8. Temperature profile $T(x,t)$ for various values of (a) P_r and (b) H.

As the heat generation parameter H increases, internal energy production within the fluid rises due to mechanisms such as chemical reactions, thermal radiation, or Joule heating. Consequently, the fluid temperature increases, thus enhancing the buoyancy-driven flow and modifying the thermal profile. Heat generation plays a significant role in industrial cooling systems, nuclear reactors, and combustion processes, where effective thermal management is essential for maintaining efficiency and operational safety.

Figure 9(a) illustrates the effect of the Schmidt number (S_c) on the concentration profile $C(x,t)$. Higher values of Sc correspond to lower mass diffusivity, resulting in steeper concentration gradients near the surface. In contrast, lower values of S_c promote faster mass diffusion and produce a more uniform distribution of species within the fluid.

Fig. 9b examines the influence of the reaction rate parameter (S) on $C(x,t)$. An increase in S causes a more rapid depletion of reactants, leading to a sharper decline in concentration near the reactive surface. This effect is particularly important in catalytic and combustion processes, where precise control of reaction rates is necessary to improve efficiency and optimize performance.

(a) (b)

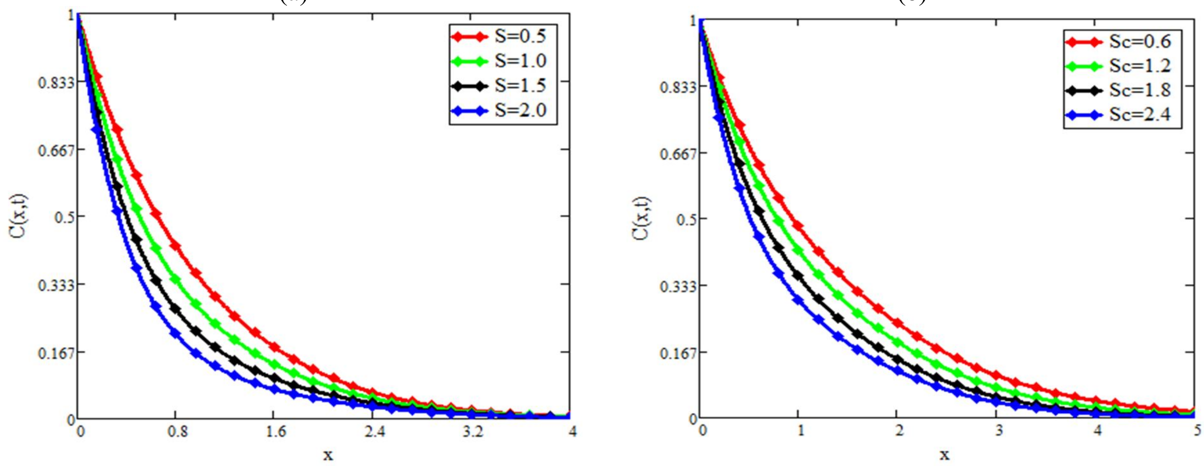

FIG. 9. Concentration profile $T(x,t)$ for various values of (a) S and (b) S_c.

This behavior is commonly observed in chemical engineering processes, pollutant dispersion, and liquid-phase mass transfer. When the Schmidt number (Sc) is low, mass diffusion occurs more rapidly, resulting in a more uniform distribution of species and reduced concentration gradients. Conversely, a higher reaction rate leads to a faster depletion of reactants, causing a sharp decline in concentration near the reactive surface. This phenomenon is particularly important in catalytic reactions, combustion processes, and industrial chemical engineering applications, where optimizing reaction rates can significantly enhance efficiency and product yield. In contrast, a lower reaction rate allows the species to persist for a longer duration, resulting in a more gradual variation in concentration.

Figure 10 presents a comparison between the results of the current study and those reported by Siyal et al. [30]. By setting $\beta = \gamma = \alpha \to 1$, $A = Sr = R = S = \lambda = 0$, and $B = \omega = 0$, the obtained results are found to be identical, thereby confirming the validity and consistency of the proposed model.

Table 1 presents a comparative validation of the present results with experimental data.

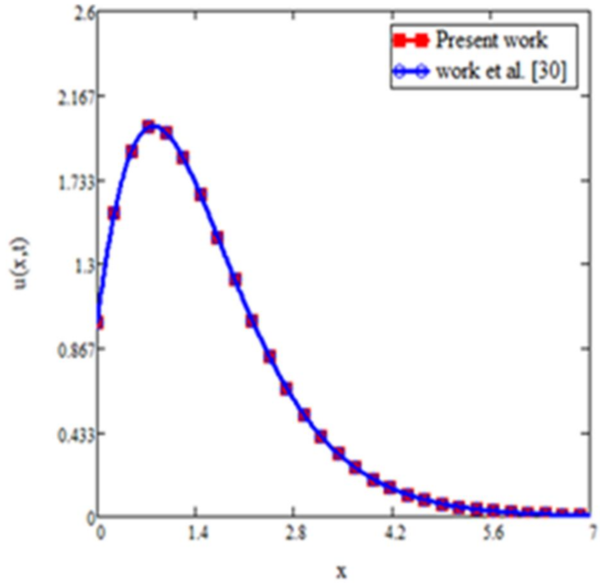

FIG. 10. Comparison of present work.

TABLE 1. Comparison of present work with previous works

Gr	Khalid et al. [12]	J.D. Olisa [19]	Present work
0.0	1.2430	1.2430	1.2431
1.0	1.4347	1.4347	1.4348
2.0	1.6252	1.6252	1.6253
3.0	1.8113	1.8113	1.8114

6. Conclusion

The study investigates the laminar flow of a Maxwell fluid over an inclined vertical surface, considering the effects of the Soret phenomenon. The governing dimensional equations are first transformed into dimensionless form and then solved using the Laplace transform method. The resulting velocity, temperature, and concentration distributions are obtained and analyzed graphically. The results indicate that increasing thermal buoyancy forces enhances the fluid velocity. Higher values of the Soret effect (thermo-diffusion) cause an increase in fluid speed, whereas a decrease in the inclination angle increases the fluid velocity. Additionally, fluid temperature decreases as the Prandtl number (Pr) increases, while stronger heat source effects increase the fluid temperature. Chemical reactions lead to a decrease in concentration, and an increase in the Schmidt number reduces the concentration profile.

References

[1] Hsiao, K.-L., Applied Thermal Engineering, 112 (2017) 1281.

[2] Shah, N.A., Vieru, D., and Fetecau, C., Journal of Magnetism and Magnetic Materials, 40, (2016) 10.

[3] Shafique, A., Nisa, Z.U., Asjad, M.I., Nazar, M., and Jarad, F., Mathematical Problems in Engineering, 2022 (2022) 279498.

[4] Shafique, A., Ramzan, M.., Ikram, Z., Amir, M., and Nazar, M., Frontiers in Heat and Mass Transfer, 20 (2023) 1.

[5] Ahmad, M., Imran, M., Aleem, M., and Khan, I., Journal of Thermal Analysis and Calorimetry, 137 (2019) 1783.

[6] Atangana, A., Akgul, A., and Owolabi, K.M., Alexandria Engineering Journal, 59 (2020) 1.

[7] Baleanu, D., Fernandez, A., and Akgul, A., Mathematics, 8 (2020) 360.

[8] Kumar, S.G., Kumar, R.K., Kumar, G.V., and Varma, S.V.K., Advanced Science, Engineering and Medicine, 8 (2016) 1.

[9] Sandeep, N. and Kumar, M.S.J., Journal of Applied Fluid Mechanics, 9 (2016) 2205.

[10] Ramzan, M., Shafique, A., Amir, M., and Nazar, M., Jordan Journal of Physics, 16 (3) (2023) 341.

[11] Ramzan, M., Nisa, Z.U., Shafique, A., and Nazar, M., Journal of Advanced Research in Fluid Mechanics and Thermal Sciences, 8 (2013) 110.

[12] Abbas, S., Ahmad, M., Nazar, M., Saleem, S., Isyanov, R., Aljedani, J., and Garalleh, H.A., Case Studies in Thermal Engineering, 2025 (2025) 105946.

[13] Abbas, S., Ramzan, M., Inam, I., Saleem, S., Nazar, M., Abduvalieva, D., and Garalleh, H.A., Scientific Reports, 14 (1) (2024) 22507.

[14] Abbas, S. and Nazar, M., Mathematical Methods in the Applied Sciences, 47 (2024) 1.

[15] Fetecau, C. and Fetecau, C., International Journal of Engineering Science, 43 (2005) 781.

[16] Ahmed, M.A.M., Mohammed, M.E., and Khidir, A.A., Propulsion and Power Research, 4 (2015) 105.

[17] Narayana, P.V.S., Propulsion and Power Research, 4 (2015) 150.

[18] Nadeem, S., Mehmood, R., and Akbar, N.S., The European Physical Journal, 129 (2014) 182.

[19] Olisa, J.D., The International Journal of Engineering and Science, 4 (2017) 08.

[20] Khan, A., Khan, I., Ali, F., and Shafie, S., Mathematical Problems in Engineering, 2014 (2014) 1.

[21] Seth, G.S., Singha, A.K., and Sharma, R., Indian Journal of Scientific Research and Technology, 3 (2015) 10.

[22] Tran, M.D., Ho, V., and Van, H.N., Mathematical Problems in Engineering, 2020 (2020) 1.

[23] Tuan, N.H., Mohammadi, H., and Rezapour, S., Chaos Solitons Fractals, 140 (2020) 1.

[24] Shateyi, S. and Motsa, S., Advanced Topics in Mass Transfer, 2011 (2011) 145.

[25] Ramzan, M., Nazar, M., Nisa, Z.U., Ahmad, M., and Shah, N.A., Mathematical Methods in the Applied Sciences, 2021 (2021) 1.

[26] Khan, Z.A., Haq, S.U., Khan, T.S., Khan, I., and Tlili, I., Results in Physics, 9 (2018) 1602.

[27] Ali, F., Khan, I., Shafie, S., and Musthapa, N., Mathematical Problems in Engineering, 3 (2013) 1.

[28] Ramzan, M., Nisa, Z.U., Ahmad, M., and Nazar, M., Complexity, 2021 (2021) 1.

[29] Khalid, A., Khan, I., and Shafie, S., The International Journal of Engineering and Science, 6 (2015) 08.

[30] Siyal, A., Abro, K.A., and Solangi, M.A., Journal of Thermal Analysis and Calorimetry, 136 (2019) 2295.

[31] Shah, N.A., Khan, I., Aleem, M., and Imran, M.A., Advances in Mechanical Engineering, 11 (2019) 1.

[32] Blair, G.S. and Caffyn, J., Nature, 155 (1955) 171.

[33] Povstenko, Y., "Fractional Thermoelasticity, Solid Mechanics and Its Applications", (Springer International Publishing, 2015) 1–219.

[34] Hristov, J., "Frontiers in Fractional Calculus", (Bentham Science Publishers, 2017) 269–340.

[35] Tzou, D.Y., "Macro to Microscale Heat Transfer: The Lagging Behavior", (Taylor and Francis, 1997) 1–339.

[36] Stehfest, H., Communication of Advanced Composite Material, 13 (1970) 47.